Neuropharmacology 153 (2019) 32–40

Contents lists available at ScienceDirect

Neuropharmacology

journal homepage: www.elsevier.com/locate/neuropharm

Endocannabinoid long-term depression revealed at medial perforant path excitatory synapses in the dentate gyrus

Sara Peñasco[a,b], Irantzu Rico-Barrio[a,b], Nagore Puente[a,b], Sonia María Gómez-Urquijo[a,b], Christine J. Fontaine[c], Jon Egaña-Huguet[a,b], Svein Achicallende[a,b], Almudena Ramos[a,b], Leire Reguero[a,b], Izaskun Elezgarai[a,b], Patrick C. Nahirney[c], Brian R. Christie[c], Pedro Grandes[a,b,c,*]

[a] Department of Neurosciences, Faculty of Medicine and Nursing, University of the Basque Country UPV/EHU, E-48940, Leioa, Spain
[b] Achucarro Basque Center for Neuroscience, Science Park of the University of the Basque Country UPV/EHU, E-48940, Leioa, Spain
[c] Division of Medical Sciences, University of Victoria, Victoria, British Columbia, V8P 5C2, Canada

HIGHLIGHTS

- CB_1 receptor inhibits excitatory medial perforant path (MPP) synaptic transmission.
- MPP stimulation triggers CB_1-dependent excitatory long-term depression (eCB-eLTD).
- ~26% of the MPP excitatory terminals contain CB_1 receptors.
- eCB-eLTD is group I metabotropic glutamate receptor dependent.
- eCB-eLTD requires 2-arachydonoyl-glycerol (2-AG) synthesis.

ARTICLE INFO

Keywords:
CB_1 receptor
2-AG
Electrophysiology
Excitatory synapses
Long-term depression
Hippocampus

ABSTRACT

The endocannabinoid system modulates synaptic plasticity in the hippocampus, but a link between long-term synaptic plasticity and the type 1 cannabinoid (CB_1) receptor at medial perforant path (MPP) synapses remains elusive. Here, immuno-electron microscopy in adult mice showed that ~26% of the excitatory synaptic terminals in the middle 1/3 of the dentate molecular layer (DML) contained CB_1 receptors, and field excitatory postsynaptic potentials evoked by MPP stimulation were inhibited by CB_1 receptor activation. In addition, MPP stimulation at 10 Hz for 10 min triggered CB_1 receptor-dependent excitatory long-term depression (eCB-eLTD) at MPP synapses of wild-type mice but not on *CB_1*-knockout mice. This eCB-eLTD was group I mGluR-dependent, required intracellular calcium influx and 2-arachydonoyl-glycerol (2-AG) synthesis but did not depend on *N*-methyl-*d*-aspartate (NMDA) receptors. Overall, these results point to a functional role for CB_1 receptors with eCB-eLTD at DML MPP synapses and further involve these receptors in memory processing within the adult brain.

1. Introduction

The hippocampus is engaged in the processing of declarative/explicit memories (Aggleton and Brown, 1999; Eichenbaum, 2000; Eichenbaum et al., 2012; Eichenbaum and Fortin, 2005), and is a key component for regulation of cognitive-related behaviors and long-term memory processing. The endocannabinoid (eCB) system collectively plays a crucial role in long-term synaptic plasticity in the hippocampus and throughout the brain, and underlies learning and memory formation (Azad et al., 2004; Castillo et al., 2012; Chevaleyre and Castillo, 2004; Chiu and Castillo, 2008; Lafourcade et al., 2007; Monday et al., 2018; Yasuda et al., 2008). Cortical inputs encoding spatial information (Aggleton and Brown, 1999; Eichenbaum, 2000; Eichenbaum et al., 2012; Reagh and Yassa, 2014) converge into the dentate gyrus (DG) via the MPP and lateral (LPP) perforant path (Hjorth-Simonsen, 1972; Hjorth-Simonsen and Jeune, 1972). The glutamatergic synapses made

* Corresponding author: Department of Neurosciences, Faculty of Medicine and Nursing, University of the Basque Country (UPV/EHU), Barrio Sarriena s/n, E-48940, Leioa, Spain.
E-mail address: pedro.grandes@ehu.eus (P. Grandes).

https://doi.org/10.1016/j.neuropharm.2019.04.020
Received 12 January 2019; Received in revised form 28 March 2019; Accepted 18 April 2019
Available online 22 April 2019

by the MPP with the granule cell dendritic spines in the middle 1/3 of the DML (Grandes and Streit, 1991) are capable of sustaining long-term depression (Christie and Abraham, 1994), show paired-pulse depression at low stimulus intensities (Petersen et al., 2013) and exhibit distinct forms of eCB-dependent synaptic plasticity (Chávez et al., 2010).

The eCB system is formed by multiple components, including cannabinoid receptors (mostly CB_1, also CB_2 and others), endocannabinoids (e.g. 2-AG and anandamide (AEA)), their synthesizing enzymes (diacylglycerol lipase (DAGL) for 2-AG and *N*-acyl phosphatidylethanolamine phospholipase D for AEA), the degrading enzymes (monoacylglycerol lipase (MAGL) for 2-AG and fatty acid amide hydrolase (FAAH) for AEA) and their transport proteins (Katona and Freund, 2012; Lutz et al., 2015; Pertwee, 2015; Piomelli, 2003). It is known that activation of the calcium-selective postsynaptic transient receptor potential vanilloid 1 (TRPV1) receptor at MPP-granule cell synapses suppresses excitatory transmission, and brief postsynaptic depolarizations (1 Hz) induce AEA-mediated TRPV1-LTD in a CB_1 receptor-independent manner (Chávez et al., 2010). These findings are in support of studies showing there is a high TRPV1 concentration in the postsynaptic dendritic spines of asymmetric perforant path synapses in the outer 2/3 of the DML (Puente et al., 2015). Interestingly, postsynaptic depolarization of DG granule cells can result in eCB release that suppresses glutamatergic inputs in the innermost 1/3 DML (Chiu and Castillo, 2008) where the CB_1 receptor-containing commissural/associational glutamatergic synapses converge (Gutiérrez-Rodríguez et al., 2017; Katona et al., 2006; Uchigashima et al., 2011). However, the same depolarization protocol does not have any effect on the excitatory synapses of the entorhinal-dentate pathway (Chiu and Castillo, 2008).

Although CB_1 receptors are expressed in the excitatory pathways of the hippocampus (Bonilla-Del Río et al., 2019; Gutiérrez-Rodríguez et al., 2017; Hu and Mackie, 2015; Katona et al., 2006; Katona and Freund, 2012; Kawamura et al., 2006; Marsicano and Lutz, 1999; Monory et al., 2006; Ruehle et al., 2013; Uchigashima et al., 2011), it still remains unclear what role the CB_1 receptor might have in long-term synaptic plasticity at MPP synapses. In this study, we addressed this question and discovered eCB-eLTD at the MPP synapses that correlates with the subcellular localization of presynaptic CB_1 receptors at these glutamatergic synapses.

2. Materials and methods

2.1. Animals

Experiments were performed on 11–12 week old male c57BL/6J mice (Janvier Labs, Le Genest-Saint-Isle, France), global CB_1 receptor knockout (CB_1-KO) mice and their wild-type (CB_1-WT) littermates. The animals were housed in pairs of littermates in standard Plexiglas cages (17 cm × 14.3 cm x 36.3 cm) and allowed to habituate to the environment for at least 1 week before experimental procedures were initiated. All animals were maintained at approximately 22 °C with a 12:12 h light:dark cycle (red light on at 9:00 a.m.). Mice had *ad libitum* access to food and water throughout all experiments. The protocols for animal care and use were approved by the Committee of Ethics for Animal Welfare of the University of the Basque Country (CEEA/M20/2016/073; CEIAB/2016/074) and were in accordance to the European Communities Council Directive of 22nd September 2010 (2010/63/EU) and Spanish regulations (Real Decreto 53/2013, BOE 08-02-2013). Great efforts were made in order to minimize the number and suffering of the animals used.

2.2. Slice preparation

Mice were anesthetized with isoflurane (2–4%) and brains were rapidly removed and placed in a sucrose-based solution at 4 °C that contained (in mM): 87 NaCl, 75 sucrose, 25 glucose, 7 $MgCl_2$, 2.5 KCl, 0.5 $CaCl_2$ and 1.25 NaH_2PO_4. Coronal vibratome sections (300 μm thick, Leica Microsistemas S.L.U.) were collected, recovered at 32–35 °C before being placed in the recording chamber, and superfused (2 ml/min) with artificial cerebrospinal fluid (aCSF) containing (in mM): 130 NaCl, 11 glucose, 1.2 $MgCl_2$, 2.5 KCl, 2.4 $CaCl_2$, 1.2 NaH_2PO_4 and 23 $NaHCO_3$, equilibrated with 95% O_2/5% CO_2. All experiments were carried out at 32–35 °C. Picrotoxin (PTX; 100 μM, Tocris Bioscience UK) was added to the aCSF in some experiments to block $GABA_A$ receptors.

2.3. Extracellular field recordings

For extracellular field recordings, a glass recording pipette was filled with aCSF. The stimulation electrode (borosilicate glass capillaries, Harvard apparatus UK capillaries 30–0062 GC100T-10) was placed in the MPP or mossy cell fibers (MCF) and the recording pipette in the middle 1/3 of the DML. To evoke field excitatory postsynaptic potential responses (fEPSPs), repetitive control stimuli were delivered at 0.1 Hz (Stimulus Isolater ISU 165, Cibertec, Spain; controlled by a Master-8, A.M.P.I.). An Axopatch-200B (Axon Instruments/Molecular Devices, Union City, CA, USA) was used to record the data filtered at 1–2 kHz, digitized at 5 kHz on a DigiData 1440A interface collected on a PC using Clampex 10.0 and analyzed using Clampfit 10.0 (all obtained from Axon Instruments/Molecular Devices, Union City, CA, USA). At the start of each experiment, an input-output curve was constructed. Stimulation intensity was selected for baseline measurements that yielded between 40 and 60% of the maximal amplitude response. To induce eCB-eLTD of glutamatergic inputs, a low frequency stimulation (LFS, 10 min at 10 Hz) protocol was applied following recording of a steady baseline as described previously (Puente et al., 2011).

The magnitude of the fEPSP area for eCB-eLTD was calculated as the percentage change between baseline area (averaged excitatory responses for 10 min before LFS) and last 10 min of stable responses, recorded 30 min after the end of the LFS. At least 3 mice were used for each experimental condition. Control mice were always intermixed with the drug groups. The paired-pulse ratio (PPR) was calculated by averaging the ratio of the fEPSP initial slopes (P2/P1) of 30 pairs of pulses (50 msec interpulse interval), where P2 corresponded to fEPSP2 slopes (2nd evoked responses) and P1 to fEPSP1 slopes (1st evoked responses).

2.4. Data analysis

All values are given as mean ± standard error of the mean (S.E.M) with p values and sample size (n). Shapiro-Wilk test and Kolmogorov-Smirnov was used to confirm normality of the data. In general, statistical significance between conditions (baseline versus after drug or stimulation protocol or both) was tested using parametric (two-tailed Student's t-test) or non-parametric (Mann-Whitney test) or one-way analysis of variance (ANOVA) with drug treatment as between group factor with subsequent post hoc analysis (Duns post test). The significance level was set at $p < 0.05$ for all comparisons. All statistical tests were performed with GraphPad Prism (GraphPad Prism 5, GraphPad Software Inc, San Diego, USA; RRID:SCR_002798).

2.5. Electron microscopy

A pre-embedding silver-intensified immunogold method was used for the localization of the CB_1 receptor protein at MPP synapses in the DML (Gutiérrez-Rodríguez et al., 2017). Adult CB_1-WT and CB_1-KO animals (n = 3, postnatal day 76) were deeply anesthetized with ketamine/xylazine (80/10 mg/kg body weight), perfused through the heart with phosphate buffered saline (PBS, 0.1 M, pH 7.4, 23 °C). They were then fixed with 250 ml of formaldehyde (4%, freshly depolymerized from paraformaldehyde), 0.2% picric acid, and 0.1% glutaraldehyde in phosphate buffer (PB; 0.1 M, pH 7.4) prepared at 4 °C. Coronal hippocampal sections cut at 50 μm on a vibratome were

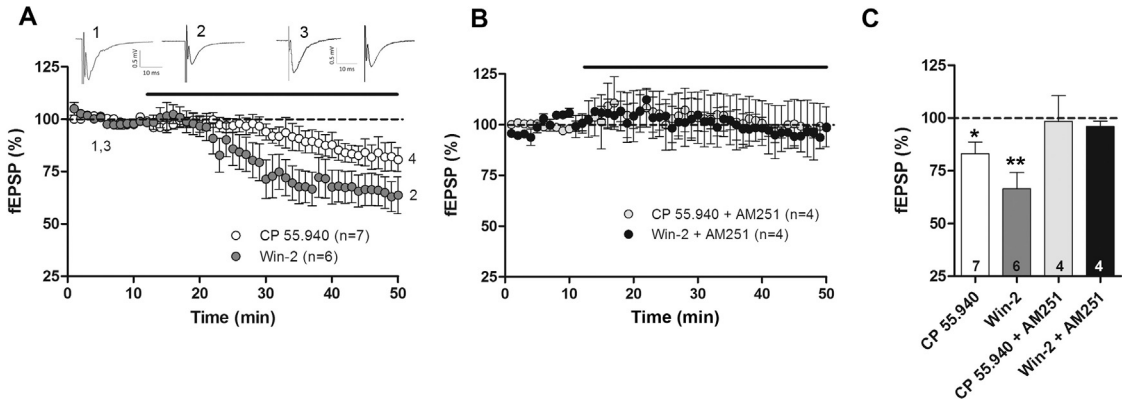

Fig. 1. eCB CB_1 receptor pharmacology on excitatory synaptic transmission at MPP synapses. (A) Time course plot showing average of fEPSP areas. The CB_1 receptor agonists (CP 55.940 10 μM; white circles and Win-2 5 μM; light gray circles) reduce fEPSP (versus baseline). **(B)** Simultaneous application of CP 55.940 (10 μM; dark gray circles) and a selective CB_1 receptor antagonist (AM251; 4 μM) inhibits the synaptic depression observed in **A** (versus baseline). Black horizontal bars on top indicate time exposure to drugs. **(C)** Summary bar histogram comparing experiments performed with CP 55.940 (10 μM), Win-2 (5 μM) and CP 55.940 + AM251 cocktail (10 μM + 4 μM, respectively). Dotted line indicates baseline prior to drug application. Numbers in the bars are individual experiments. One-way ANOVA ($F_{3,33}$ = 11.52, ***p < 0.001) and Dunn's Multiple Comparison Test (*p < 0.05; ***p < 0.001; p > 0.05 versus baseline, respectively). Data expressed as mean ± S.E.M.

collected in 0.1 M PB (pH 7.4) at room temperature (RT). Sections were pre-incubated in a blocking solution of 10% bovine serum albumin (BSA), 0.02% saponin and 0.1% sodium azide in Tris-HCl buffered saline (TBS, pH 7.4) for 30 min at RT. The sections were then incubated with goat polyclonal *anti*-CB_1 receptor antibody (2 μg/ml, #CB1-Go-Af450, Frontier Science Co.;RRID: AB_257130) in 10% BSA/TBS with 0.004% saponin and 0.1% sodium azide, on a shaker for 2 days at 4 °C. After five washes in 1% BSA/TBS (3 × 1 min and 2 × 10 min), they were incubated with 1.4 nm gold-conjugated rabbit anti-goat IgG (Fab' fragment, 1:100, Nanoprobes Inc., Yaphank, NY, USA) in 1% BSA/TBS with 0.004% saponin on a shaker for 4 h at RT. After three washes in 1% BSA/TBS (10 min each), the tissue was kept in 1% BSA/TBS overnight at 4 °C, then post-fixed in 1% glutaraldehyde in TBS for 10 min and washed three times in double-distilled water (10 min each). Nanogold particles were silver-intensified with a HQ Silver kit (Nanoprobes Inc., Yaphank, NY, USA) for 12 min in the dark and then washed three times in double distilled water (1 min each) and three times in 0.1 M PB (10 min each). Immunolabeled sections were osmicated (1% OsO_4 (v/v) in 0.1 M PB, 20 min), dehydrated in graded alcohols to propylene oxide and plastic-embedded in Epon resin 812. Ultrathin sections (50 nm) were placed on nickel mesh grids, stained with 2.5% lead citrate for 20 min, and then examined with a Philips EM208S transmission electron microscope. Sections were imaged with a digital camera (Digital Morada Camera, Olympus) and saved as tif files. Adjustments in contrast and brightness were made to the figures using Adobe Photoshop (Adobe Systems, San Jose, CA, USA; RRID:SCR_014199).

2.6. Semi-quantification analysis

To ensure an accurate comparison between conditions, the pre-embedding immunogold method was applied simultaneously to the hippocampal sections collected from the animals studied (n = 3 for each condition). Labeled sections were examined under a light microscope in order to select portions of the middle 1/3 of the DML with conspicuous and reproducible CB_1 receptor immunolabeling. To avoid false negatives, only ultra-thin sections within the first 1.5 μm from the surface of the tissue block were examined. All electron micrographs were taken at 18,000× magnification and metal particles on membranes were visualized and counted. Positive labeling was considered if at least one immunogold particle was within 30 nm from the membrane of the specific compartment under study. Image-J (NIH, USA; RRID:SCR_003070) was used to measure the membrane length. Sampling was always carefully and accurately carried out in the same way for all the animals studied, and experimenters were blinded to the condition of the subject for CB_1 receptor quantification.

A total of 328 excitatory synapses in *CB_1*-WT and 79 excitatory synapses in *CB_1*-KO mice were measured. Percentages of CB_1 receptor positive profiles, density (particles/μm membrane) of CB_1 receptor immunoparticles in presynaptic terminals and proportion of CB_1 receptor immunoparticles in different compartments versus total CB_1 receptor expression in cell membranes were determined and displayed as mean ± S.E.M. using a statistical software package (GraphPad Prism, San Diego, USA; RRID:SCR_002798). A normality test (Kolmogorov-Smirnov) was applied before running further statistical tests. Data were analyzed using a nonparametric Kruskal-Wallis test.

2.7. Drugs and chemicals

All drugs used in the electrophysiological experiments were dissolved in dimethyl sulfoxide (DMSO; Sigma-Aldrich) and added at the final concentration to the superfusion medium.

3. Results

3.1. CB_1 receptor-mediated inhibition of excitatory synaptic transmission at the MPP-granule cell synapses

Direct activation of CB_1 receptors in the DG by the CB_1 agonists CP 55.940 (10 μM) or Win-2 (5 μM) in the presence of PTX (100 μM) resulted in a reduction in excitatory synaptic transmission at MPP-granule cell synapses (Fig. 1A and C). The area of the fEPSP was reduced significantly in both conditions (CP 55.940: 83.03 ± 5.67% fEPSP; n = 7; *p < 0.05 versus baseline; Win-2: 66.55 ± 7.53% fEPSP; n = 6; ***p < 0.001 versus baseline). This depression of the fEPSP was mediated by CB_1 receptors, as it could be prevented by co-perfusion with the selective CB_1 receptor antagonist AM251 (4 μM; 98.47 ± 12.15% fEPSP; n = 4; p > 0.05 versus baseline; Fig. 1B–C).

3.2. Excitatory LTD at dentate MPP-granule cell synapses

We have previously reported that LFS at 10 Hz for 10 min induces eCB-eLTD in the extended amygdala (Puente et al., 2011). In the current study, we applied similar stimulation in the presence of PTX and found that this induced a long-lasting depression at the MPP-granule cell synapses (16.50 ± 5.75% depression; n = 20; **p < 0.01 versus

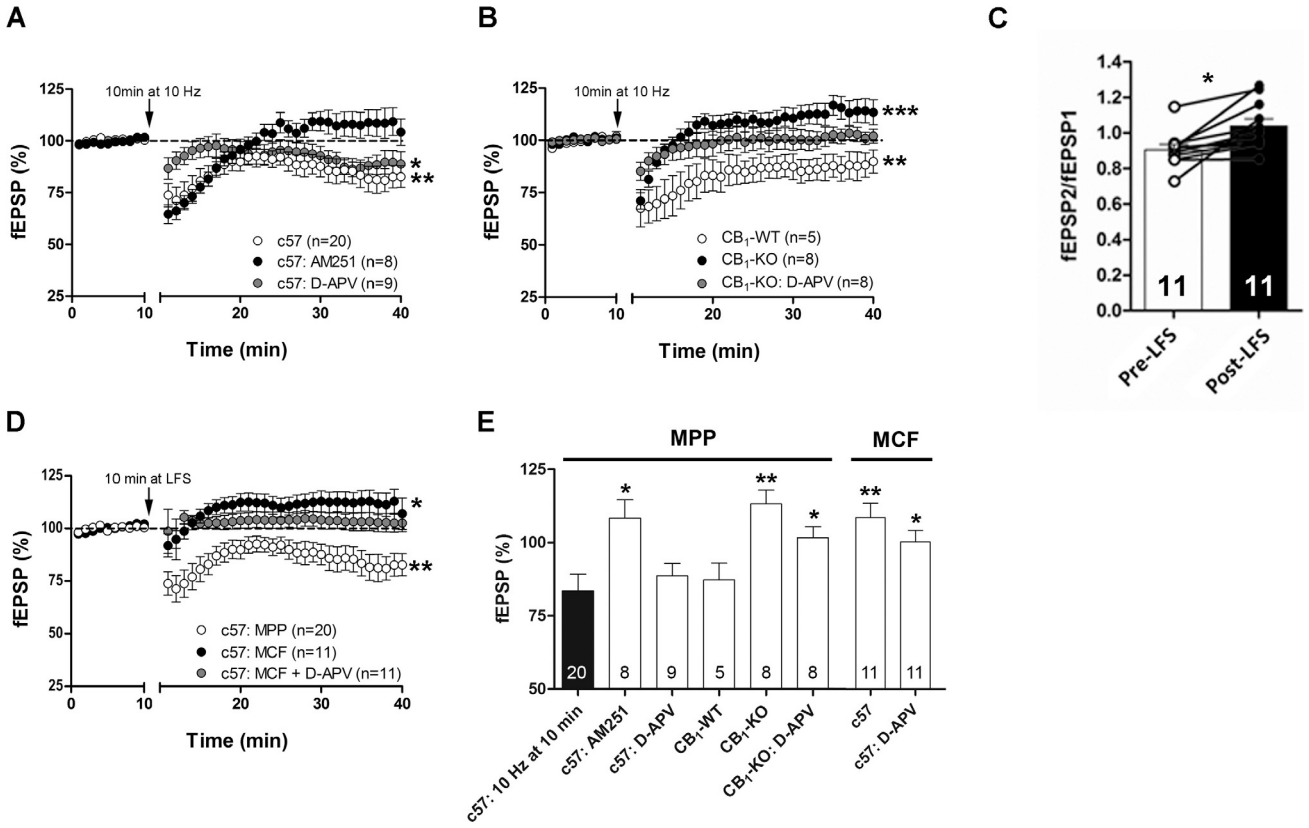

Fig. 2. eCB-dependent LTD at MPP synapses. (A) LFS (10 Hz for 10 min) at the time marked by the X-axis break triggers eCB-eLTD at MPP synapses (white circles; Student's *t*-test, two tailed, $t_{38} = 2.89$; $^{**}p < 0.01$ versus baseline). While AM251 (4 μM) inhibits eCB-eLTD (black circles; Student's *t*-test, two tailed, $t_{14} = 1.39$; $p > 0.05$ versus baseline), the NMDA receptor antagonist D-APV (50 μM) is ineffective (gray circles; Student's *t*-test, two tailed, $t_{16} = 2.68$; $^{*}p < 0.05$ *vs.* baseline). **(B)** eCB-eLTD is induced in *CB*$_1$-WT littermate mice (white circles; Mann Whitney test; $^{**}p < 0.01$ versus baseline) but not in *CB*$_1$-KO mice (black circles; Mann Whitney test; $^{***}p < 0.001$ versus baseline). The slight but significant LTP in *CB*$_1$-KO is suppressed by D-APV (50 μM; gray circles; Mann Whitney test; $p > 0.05$ versus baseline). **(C)** PPR was calculated from the slopes of 30 sweeps (i.e. 10 min before and 20 min after stimulation protocol). PPR is augmented after LFS (Post-LFS). Student's *t*-test, two tailed, $t_{20} = 2.63$; $^{*}p < 0.05$ versus Pre-LFS. Numbers in the bars are individual experiments. **(D)** LFS (10 Hz for 10 min) induces a slight LTP at MCF synapses in the inner 1/3 of the DML (black circles; Student's *t*-test, two tailed, $t_{20} = 2.31$; $^{*}p < 0.05$ versus baseline) which is inhibited by D-APV (50 μM; grey circles; Student's *t*-test, two tailed, $t_{20} = 0.73$; $p > 0.05$ versus baseline). **(E)** Summary bar histogram of the experiments performed: c57, AM251 (4 μM), D-APV (50 μM), *CB*$_1$-WT, *CB*$_1$-KO and *CB*$_1$-KO + D-APV (50 μM) in MPP, c57 and D-APV (50 μM) in MCF. One-way ANOVA ($F_{8,84} = 5.37$, $^{***}p < 0.001$) and Bonferroni's Multiple Comparison Test ($p > 0.05$; $^{*}p < 0.05$; $^{**}p < 0.01$ versus c57). Numbers in the bars are individual experiments. Data are expressed as mean ± S.E.M.

baseline; Fig. 2A). This LTD could be inhibited by including AM251 (4 μM) in the aCSF but was not by the NMDA receptor antagonist D-APV (50 μM; Fig. 2A and E). When these same stimuli were applied in recordings made from global *CB*$_1$-KO mice, the 10 Hz stimuli failed to induce eCB-eLTD (Fig. 2B and E). Rather, in these mice the 10 Hz stimulation produced a slight potentiation (13.14 ± 4.81% potentiation; n = 8; $^{***}p < 0.01$ versus baseline; Fig. 2B) that was reduced to baseline levels by perfusion with D-APV (50 μM; 1.74 ± 3.72% potentiation; n = 8; $p > 0.05$ versus baseline; p > 0.05 versus potentiation value from *CB*$_1$-KO; Fig. 2B and E).

In contrast to the results obtained in the DML, application of the 10 Hz stimulation at MCF synapses did not induce eCB-eLTD (11.82 ± 5.11% potentiation; n = 11; $^{**}p < 0.01$ versus MPP eCB-eLTD; Fig. 2D) as previously shown by Chiu and Castillo (2008). The small potentiation that was observed at these synapses (11.82 ± 5.11% potentiation; $^{*}p < 0.05$ versus baseline; Fig. 2D) was reduced to baseline levels by the perfusion with D-APV (3.07 ± 4.15% potentiation; n = 11; $p > 0.05$ versus baseline; $p > 0.05$ versus potentiation value from MCF; Fig. 2D and E). Together, these results demonstrate that the 10 Hz stimuli are able to induce eCB-eLTD not previously reported at MPP-granule cell synapses.

3.3. eCB-eLTD mechanisms at MPP-granule cell synapses

To determine if eCB-eLTD has a presynaptic or postsynaptic loci we examined the PPR prior to, and following, the induction of eCB-eLTD. We found that eCB-eLTD involves the suppression of presynaptic transmitter release, since there was a significant increase in the PPR following the application of the 10 Hz stimuli (1.04 + 0.04; n = 11; $^{*}p < 0.05$ versus Pre-LFS; Fig. 2C).

The group I mGluR agonist 3.5-DHPG produced a significant decrease in the fEPSP of MPP in sham mice (Fig. 3A). In addition, 3.5-DHPG has previously been reported to induce LTD at CA1 synapses (Huber et al., 1998), but it is not clear whether the MPP input to the DG is capable of sustaining this form of LTD. To explore the contribution of the mGluR/phospholipase C (PLC) pathway to eCB-eLTD, the application of 3.5-DHPG (50 μM) occluded the subsequent induction of eCB-eLTD (10.54 ± 9.48% potentiation; n = 11; $^{*}p < 0.05$ versus MPP eCB-eLTD; $p > 0.05$ versus baseline; Fig. 3B and D). In addition, eCB-eLTD could also be inhibited by administration of either the mGluR5 antagonist MPEP (10 μM; 14.20 ± 10.54% potentiation; n = 13; $^{*}p < 0.05$ versus MPP eCB-eLTD; $p > 0.05$ versus baseline; Fig. 3C–D) or the mGluR1 antagonist CPCCoEt (50 μM; 9.48 ± 6.69% potentiation; n = 10; $^{**}p < 0.01$ versus MPP eCB-eLTD; $p > 0.05$ versus baseline; Fig. 3C–D). Endocannabinoids have been shown to suppress

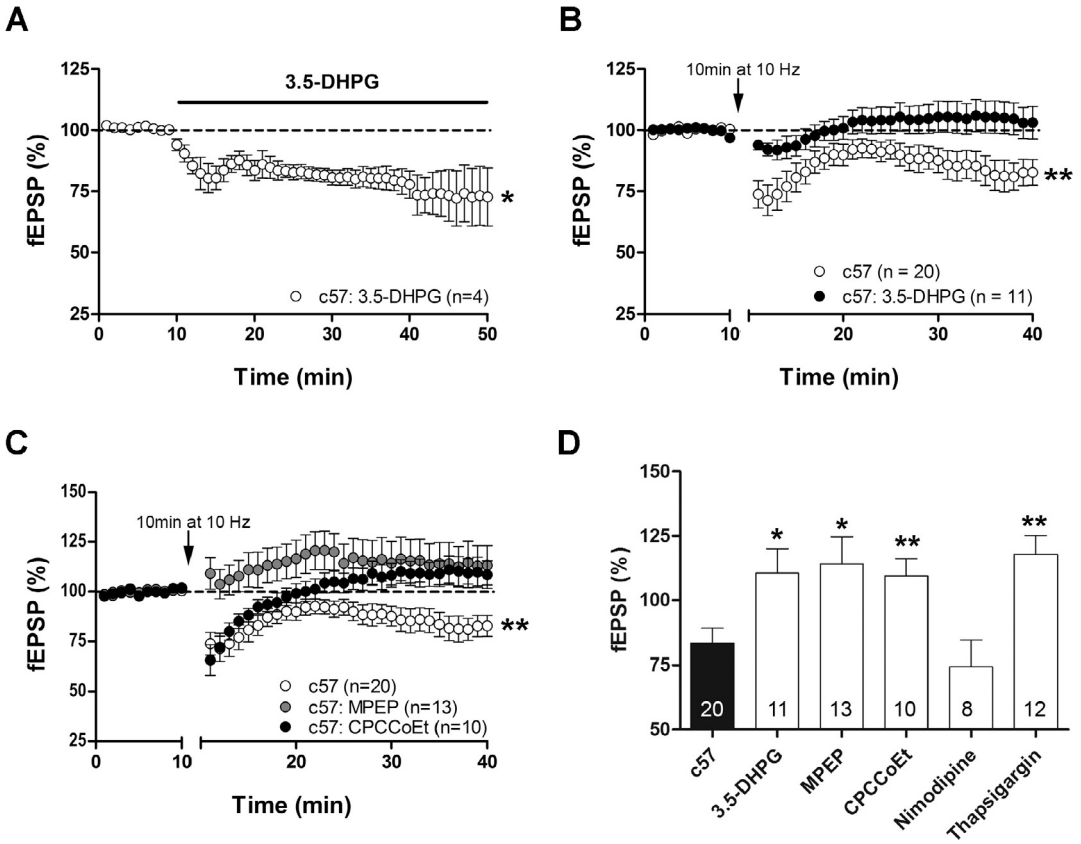

Fig. 3. Activation of group I mGluRs and calcium from intracellular stores are required for eCB-eLTD at MPP synapses. The average of the fEPSP areas is shown. **(A)** The group I mGluR agonist 3.5-DHPG reduces fEPSPs (white circles; Mann Whitney test; $*p < 0.05$ versus baseline). **(B)** eCB-eLTD elicited by LFS (white circles) is prevented by co-application of 3.5-DHPG (50 μM; black circles; Student's *t*-test, two tailed, $t_{20} = 0.74$; $p > 0.05$ versus baseline). **(C)** The mGluR5 antagonist MPEP (10 μm; grey circles; Mann Whitney test; $p > 0.05$ versus baseline) and the mGluR1 antagonist, CPCCoEt (50 μM; black circles; Mann Whitney test; $p > 0.05$ versus baseline), inhibit eCB-eLTD (white circles; Student's *t*-test, two tailed, $t_{38} = 2.89$; $**p < 0.01$ versus baseline). **(D)** Summary bar histogram of the experiments performed: c57, 3.5-DHPG (50 μM), MPEP (10 μm), CPCCoEt (50 μM), nimodipine (1 μM), thapsigargin (2 μM, > 1 h). Mann Whitney test; $p > 0.05$; $*p < 0.05$; $**p < 0.01$ versus c57. Numbers in the bars are individual experiments. Data expressed as mean ± S.E.M.

neurotransmitter release when they are released following a depolarization that increases intracellular calcium levels (Brenowitz and Regehr, 2003) or by activation of the G-protein coupled mGluR/PLC pathway to produce diacylglycerol (DAG, Yoshida et al., 2006). We found that the inclusion of thapsigargin (2 μM), a sarco/endoplasmic reticulum Ca^{2+}-ATPase pump blocker in the aCSF was able to block eCB-eLTD (17.88 ± 7.35% potentiation; n = 12; $**p < 0.01$ versus MPP eCB-eLTD; Fig. 3D) suggesting a role for intracellular calcium in eCB-eLTD. However, calcium influx from L-type voltage-gated calcium channels is not involved in this eCB-eLTD, since the inclusion of nimodipine (1 μM) in the aCSF did not block eCB-eLTD (25.65 ± 10.20% depression; n = 8; $p > 0.05$ versus MPP eCB-eLTD; Fig. 3D). Together, these data indicate that the activation of group I mGluRs and intracellular calcium release are necessary for eCB-eLTD at MPP-granule cell synapses.

The 10 Hz stimuli were also applied in the presence of the DAGL inhibitors tetrahydrolipstatin (THL, 10 μM) or RHC-80267 (100 μM). In both conditions, eCB-eLTD was completely abolished (THL: 14.17 ± 7.31% potentiation; n = 7; $**p < 0.01$ versus MPP eCB-eLTD; RHC-80267: 11.12 ± 6.16% potentiation; n = 4; $*p < 0.05$ versus MPP eCB-eLTD; Fig. 4A and C). Also, the PLC inhibitor U73122 (5 μM) blocked eCB-eLTD (18.56 ± 6.15% potentiation; n = 6; $**p < 0.01$ versus MPP eCB-eLTD; Fig. 4C). These data suggest that PLC activity is required for 2-AG synthesis and the induction of eCB-eLTD. Furthermore, the MAGL inhibitor JZL184 (50 μM) also blocked the eCB-eLTD (6.93 ± 3.54% potentiation; n = 12; $**p < 0.01$ versus MPP eCB-eLTD; Fig. 4C) suggesting that 2-AG regulation may be a limiting factor for eCB-eLTD induction, since JZL184 reduced the fEPSP area by its own (75.74% ± 14.13% of depression; n = 6. Data not shown). Consequently, CB_1 receptor desensitization caused by a high 2-AG concentration and the long JZL184 incubation time before recordings (Fig. 4C) could be responsible for the eCB-eLTD blockade. In this line, previous studies have shown that a long-term increase in 2-AG elicits CB_1 receptor desensitization (Chanda et al., 2010; Schlosburg et al., 2010). By contrast, eCB-eLTD was unaffected by the potent and selective FAAH inhibitor URB 597 (2 μM; 18.14 ± 8.52% depression; n = 10; $p > 0.05$ versus MPP eCB-eLTD; $*p < 0.05$ versus baseline; Fig. 4B–C) indicating that AEA is not involved in the eCB-eLTD at the MPP-granule cell synapses.

3.4. Subcellular localization of CB_1 receptors at MPP terminals in the DG

CB_1 receptor immunogold particles in the middle 1/3 of the DML were localized to inhibitory and excitatory axon terminals forming synapses with dendrites and dendritic spines, respectively, and several other cell compartments (Fig. 5). The proportion of the total CB_1 receptor gold particle distribution was determined in excitatory terminals (12.03 ± 0.91%), inhibitory terminals (54.90 ± 2.18%), mitochondria (8.72 ± 0.22%), dendrites (10.39 ± 1.90%) and other membranes (13.94 ± 1.03%; Fig. 5D). Furthermore, 26.31 ± 1.19% of the excitatory terminals were CB_1 receptor-positive with a density of 0.64 ± 0.04 CB_1 receptor particles/μm. CB_1 receptor immunolabeling was absent in the *CB_1*-KO mice ($***p < 0.001$ versus WT; Fig. 5 E-G).

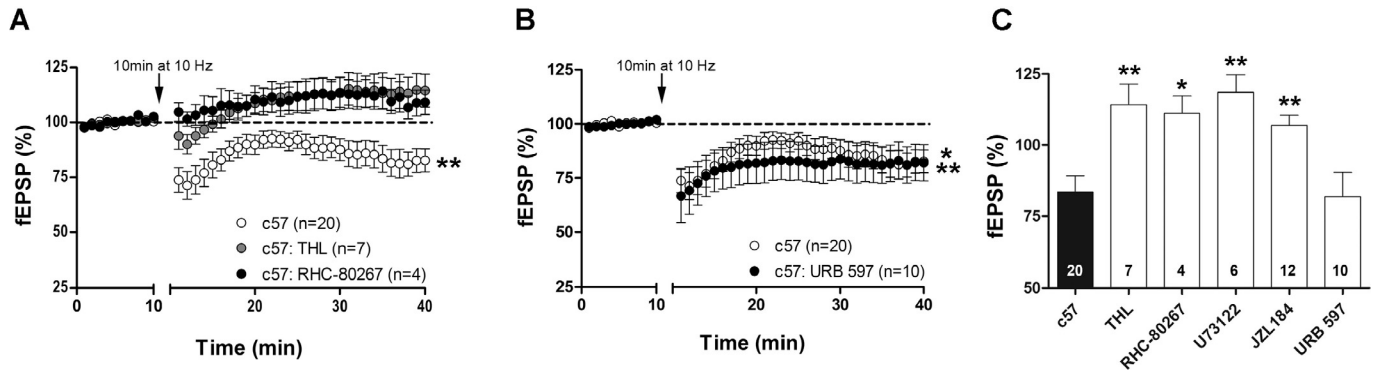

Fig. 4. 2-AG is necessary for eCB-eLTD at MPP synapses. The average of the fEPSP area is shown. **(A)** eCB-eLTD (white circles) is abolished by the DAGL inhibitors THL (10 μM; grey circles; Student's *t*-test, two tailed, $t_{12} = 1.93$; $p > 0.05$ versus baseline) and RHC-80267 (100 μM; black circles: Mann Whitney test; $p > 0.05$ versus baseline, respectively). **(B)** The FAAH inhibitor URB 597 (2 μM, > 20 min; black circles) is ineffective at eCB-eLTD (Student's *t*-test, two tailed, $t_{18} = 2.12$; $^{*}p < 0.05$ versus baseline). **(C)** Summary bar histogram of the experiments performed: c57, THL (10 μM), RHC-80267 (100 μM), U73122 (5 μM, > 1 h), JZL184 (50 μM, > 1 h) and URB 597 (2 μM, > 20 min). Mann Whitney test; $p > 0.05$; $^{*}p < 0.05$; $^{**}p < 0.01$ versus c57. Numbers in the bars are individual experiments. Data expressed as mean ± S.E.M.

4. Discussion

This study reveals the existence of CB_1 receptor-dependent excitatory LTD at the MPP synapses in the DG of adult c57BL/6J male mice that requires postsynaptic activation of group I mGluRs, calcium release from intracellular stores, and 2-AG synthesis acting on presynaptic CB_1 receptors localized at glutamatergic presynaptic terminals of the MPP.

4.1. Mechanisms underlying the eCB-eLTD at MPP-granule cell synapses

We found a CB_1 receptor-dependent inhibition of MPP-granule cell excitatory synaptic transmission. In addition, a LFS protocol (10 Hz for 10 min) that has previously been used to consistently induce eCB-

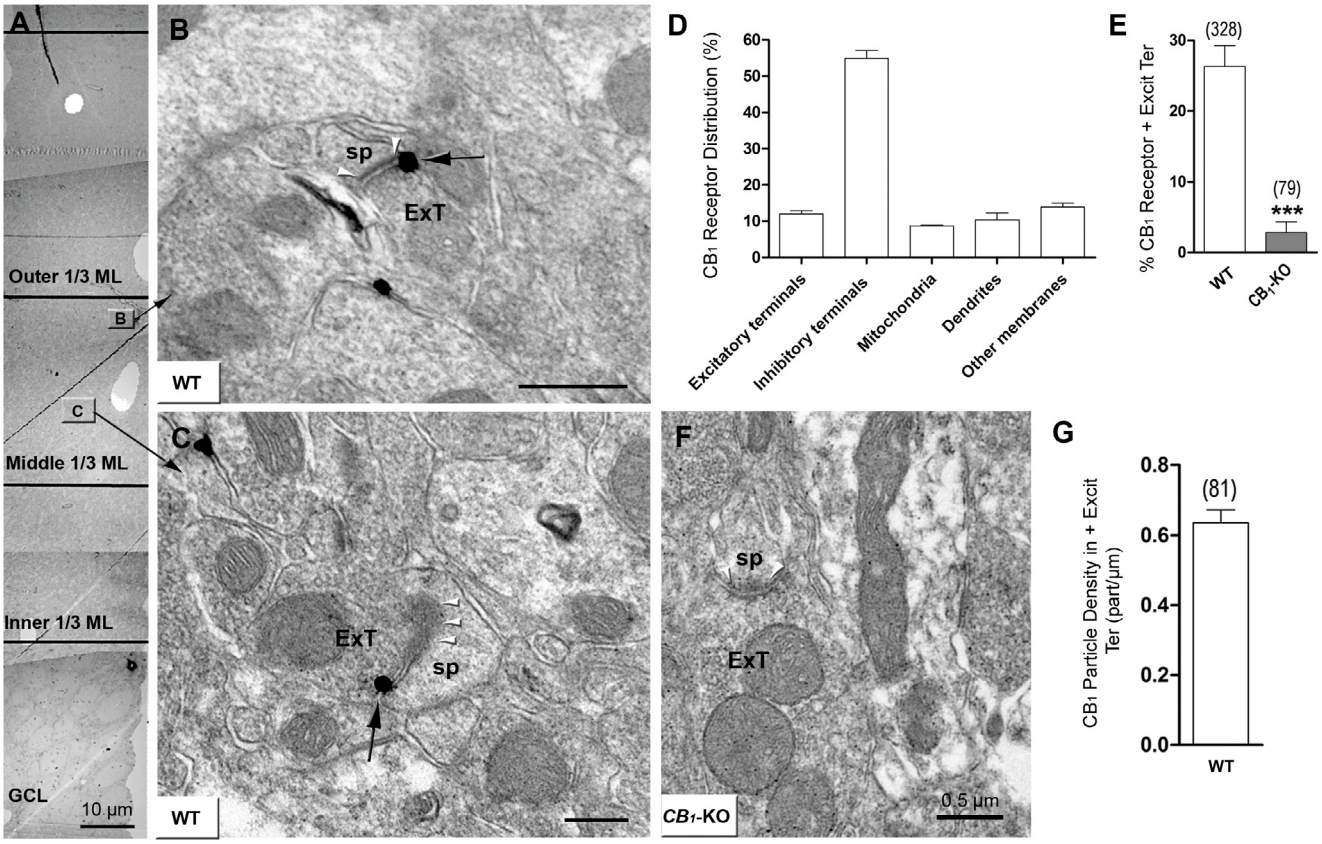

Fig. 5. Immunoelectron localization of CB_1 receptors in the middle 1/3 of the DML. (A) Reconstruction of the whole DML and granule cell layer (GCL) indicating where images shown in B and C are from. Scale bar = 10 μm. **(B, C)** CB_1 receptor immunogold labeling (arrows) is observed on presynaptic excitatory terminals (ExT) forming asymmetric synapses (arrowheads) with dendritic spines (sp). Scale bars = 0.5 μm. **(D)** Proportion of CB_1 receptor labeling in different compartments normalized to the total CB_1 receptor signal. **(E)** Percentage of CB_1 receptor-immunopositive excitatory terminals in WT and *CB_1*-KO mice. Student's *t*-test, two tailed, $t_{36} = 5.56$; $^{***}p < 0.001$ versus WT. The number of synaptic terminals analyzed is in parentheses on the top of each column. **(F)** No CB_1 receptor immunolabeling is seen in *CB_1*-KO mice. **(G)** CB_1 receptor density (particles/μm) in CB_1 receptor positive excitatory terminals. Data expressed as mean ± S.E.M. Scale bars = 0.5 μm.

dependent LTD in other brain regions (Lafourcade et al., 2007; Puente et al., 2011), elicited a eCB-eLTD at MPP synapses. We also observed that the magnitude of eCB-eLTD was unaffected by the NMDA receptor antagonist D-APV suggesting that NMDA receptors were not involved in the eCB-eLTD despite the fact that eCB-eLTD may require NMDA receptor activity at other synapses (Bender et al., 2006; Sjöström et al., 2003). Intriguingly, the slight potentiation observed in CB_1-KO mice after LFS could be triggered by the increase in glutamate release and NMDA receptor activation (Errington et al., 1987) since that potentiation disappeared after bath perfusion of D-APV. CB_1 receptors are highly expressed in the innermost 1/3 of the DML which receives excitatory inputs from hilar mossy cells (Gutiérrez-Rodríguez et al., 2017; Katona et al., 2006; Kawamura et al., 2006; Monory et al., 2006). However, consistent with a prior report (Chiu and Castillo, 2008), the stimulation protocol applied in our study was unable to induce eCB-LTD at mossy cell-granule cell synapses, but rather induced a small LTP that was inhibited by D-APV.

The stimulation paradigm could be a critical factor for the eCB-eLTD induction at the MPP-granule cell synapses. Furthermore, a TRPV1-dependent LTD at these same synapses was shown to require mGluR5 activation, but not mGluR1, and involved postsynaptic AMPA receptor internalization (Chávez et al., 2010). In our study, LFS of MPP inputs activated both mGluR1 and mGluR5 leading to an increase in intracellular calcium released from the sarco/endoplasmic reticulum. TRPV1-LTD could also be induced by stimulation at 10 Hz for 10 min in the bed nucleus of the stria terminalis (BNST) which was mediated by postsynaptic mGluR5-dependent release of AEA acting on postsynaptic TRPV1 receptors, and strongly inhibited by depletion of intracellular calcium stores (Puente et al., 2011). We found that the eCB-eLTD at MPP synapses was 2-AG dependent and activates CB_1 receptors distributed on presynaptic excitatory terminals in the middle 1/3 of the DML. In the BNST, however, dendritic L-type calcium channels and the subsequent release of 2-AG acting on presynaptic CB_1 receptors triggered retrograde short-term depression (Puente et al., 2011).

The different kinetics of recovery after LFS following MPEP and CPCCoEt suggest that mGluR5 and mGluR1 contribute differentially to the eCB-eLTD shown at the MPP-granule cell synapses. That is, while MPEP has an effect on both the induction and late phase, CPCCOEt only affects the late phase of this form of plasticity. Our results demonstrate that both mGluR5 and mGluR1 activation is critically required for persistent eCB-LTD at the MPP-granule cell synapses. However, only mGluR5, and not mGluR1, is required for the initial depression. Previous studies in the CA1 hippocampus have shown that differences between both group I mGluR subtypes have distinct effects on synaptic plasticity and memory processes (Neyman and Manahan-Vaughan, 2008). Mechanistically, the activation of mGluR1 causes an intracellular calcium rise, neuronal depolarization and increase in the frequency of spontaneous inhibitory postsynaptic potentials (Mannaioni et al., 2001). However, mGluR5 activation leads to the suppression of calcium-activated potassium currents (IAHP) and the potentiation of *Nd*NMDA receptor currents (Attucci et al., 2001; Jia et al., 1998; Mannaioni et al., 2001).

The variability observed among studies could be due to several critical factors like mouse age (PND 74–80), temperature of the *in vitro* experiments (32–35 °C) and/or the stimulation paradigm. Significantly, the eCB-LTD can be induced at either presynaptic (our work) or postsynaptic loci (Chávez et al., 2010) of the MPP-granule cell synapses depending on the stimulation, recruiting either presynaptic CB_1 receptors or postsynaptic TRPV1 and mobilizing 2-AG or AEA, respectively. Together, our findings further suggest that the precise subcellular localization of the eCB components in specific cell types and synapses are key players for the induction of diverse forms of synaptic plasticity through distinct signaling mechanisms (Castillo et al., 2012; Puente et al., 2011).

4.2. Functional context of the eCB-eLTD at MPP-granule cell synapses

Brain functions regulated by the eCB system rely on its distribution in cerebral tissue (Busquets-Garcia et al., 2018; Castillo et al., 2012; Hu and Mackie, 2015; Katona and Freund, 2012). The hippocampus is required for declarative/episodic memory and is involved in spatial and context-dependent learning (Eichenbaum et al., 2012). Inputs from the postrhinal cortex convey spatial information to the dorsolateral medial entorhinal cortex that projects to the dorsal hippocampus through the MPP (Fyhn et al., 2004; Hargreaves et al., 2005). On the other hand, the perirhinal cortex projects to the lateral entorhinal cortex which gives rise to the LPP (Burwell, 2000). The LPP pathway transmits non-spatial information, and, together with information about spatial clues forwarded by the MPP into the DG, representations for object-place or event-place scenarios are thought to be built (Gaffan, 1998; Hargreaves et al., 2005; Suzuki et al., 1997). At the same time, signal integration by granule cells related to environment or context is under control of hilar mossy cells which are critical in the learning of information sequences (Lisman et al., 2005). The mossy cells receive glutamatergic granule mossy fiber collaterals, and in turn send commissural/associational fibers that travel long distances giving innervation to multiple dentate granule cells forming mossy-granule cell synapses (Amaral and Witter, 1989; Scharfman and Myers, 2013). The glutamatergic synapses of the three excitatory pathways targeting the dentate granule cells contain CB_1 receptors (Gutiérrez-Rodríguez et al., 2017; Katona et al., 2006; Katona and Freund, 2012; Kawamura et al., 2006; Marsicano and Lutz, 1999; Monory et al., 2006; Uchigashima et al., 2011; Wang et al., 2016) and display different forms of eCB dependent-synaptic plasticity (Chávez et al., 2010; Chiu and Castillo, 2008; Wang et al., 2018, 2016) which correlate with the distinct information processed by each pathway Table 1.

As previously shown in single BNST neurons (Puente et al., 2011), either the 2-AG and CB_1 receptor-dependent eLTD herewith described, or the AEA and TRPV1-dependent eLTD at the MPP synapses (Chávez et al., 2010) might each be switched on by distinct patterns of neural activity conveying spatial information. At the same time, high frequency stimulation of the LPP in the outer 1/3 of the DML leads to 2-AG production and CB_1 receptor-dependent eLTP at these LPP synapses which have been associated with memories related to odor discrimination, and semantic information and representation (Wang et al., 2018, 2016).

Altogether, the spatial and non-spatial information transmitted by granule cells to CA3 pyramidal neurons that provides sequence learning and sequence prediction (Hunt et al., 2013) would involve perforant path inputs and different forms of cannabinoid-dependent plasticity recruited upon the type of information processed, all being modulated by mossy cell activity. Learning and memory processes that involve the hippocampus can be affected by some pathological conditions. For instance, impaired recognition, spatial, and associative memories can be observed in the adult brain after high ethanol exposure (binge drinking) during adolescence (Rico-Barrio et al., 2018). This also correlates with a decrease in CB_1 receptor expression in astrocytes (Bonilla-Del Río et al., 2019), as well as with changes in CB_1 receptor expression at the perforant path synapses (Peñasco et al., 2015). Interestingly, the memory impairment observed after adolescent binge drinking is recovered in adults exposed to enriched environmental conditions (Rico-Barrio et al., 2018). It is plausible that changes in different forms of CB_1 receptor-dependent plasticity in the DG underlie the memory deficits observed in adults after adolescent binge drinking, as well as in the distortion of space perception experienced as a psychoactive effect of cannabis use.

5. Conclusions

Field excitatory postsynaptic potentials evoked by MPP stimulation in the DML are inhibited upon CB_1 receptor activation. Second, low frequency stimulation (10 min, 10 Hz) of the MPP of adult c57BL/6J

Table 1
Different forms of eCB-mediated synaptic plasticity in the dentate gyrus.

Species	Synapse type	Induction protocol	Induction requirements	References
Rat	MCF inputs to dentate granule cells (DGC)/(MCF-DGC synapses)	Depolarization step (from −70 mV to o mV) of 3-s	eCB-DSE, calcium-dependent, modulated by cholinergic and group I mGluRs, DAGL independent	Chiu and Castillo (2008)
Rat	MCF inputs to DGC/(MCF-DGC synapses)	Theta-burst stimulation or high frequency stimulation or spike-timing dependent plasticity	No eCB-LTD	Chiu and Castillo (2008)
Rat	GABAergic inputs to DGC/(GABAergic-DGC synapses)	Depolarizing step of 1–3 s or a series of short (500 ms) repetitive depolarizations	eCB-DSI, calcium dependent, involves ryanodine receptor (RyR)-mediated Ca^{2+} release	Isokawa and Alger (2005)
Rat	GABAergic inputs to hilar mossy cells (HMC)/(GABAergic-HMC synapses)	Depolarization step of 5-s	eCB-DSI, confined to very small spaces (e.g., ≤20 μm), Ca^{2+} dependent and facilitated by activation of mAChRs	Hofmann et al. (2006)
Rat, mouse	MPP inputs to DGC/(MPP-DGC synapses)	Brief postsynaptic depolarizations (1 Hz)	Anandamide-mediated TRPV1-LTD in a CB_1 receptor-independent manner, Ca^{2+} calcineurin and clathrin-dependent internalization of AMPA receptors	Chávez et al., (2010)
Rat, mouse	LPP inputs to DGC/(LPP-DGC synapses)	2 trains of 100 Hz, each lasting 1s	2-AG-mediated CB_1-LTP via small GTPases and the assembly of latrunculin A-sensitive actin filaments	Wang et al. (2016)
Rat, mouse	LPP inputs to DGC/(LPP-DGC synapses)	1 or 2 trains of 100 Hz, lasting 1s	2-AG-mediated CB_1-LTP involving β1 integrins and presynaptic actin regulatory signaling	Wang et al. (2018)

male mice triggers eCB-eLTD at the MPP-granule cell synapses that is absent in *CB_1*-KO mice. Third, the eCB-eLTD is group I mGluR-dependent and requires intracellular calcium influx and 2-AG synthesis. This eCB-eLTD at the MPP-granule cell synapses herewith described for the first time widens the knowledge on the role of CB_1 receptors in different forms of synaptic plasticity in the brain.

Conflicts of interest

The authors declare that the research was conducted in the absence of any commercial or financial relationships that could be construed as a potential conflict of interest.

Disclosures

The authors declare that the research was conducted in the absence of any commercial or financial relationships that could be construed as a potential conflict of interest.

Acknowledgments

We thank all members of P. Grandes laboratory for their helpful comments, suggestions, and discussions during the performance of this study. The authors thank Giovanni Marsicano (INSERM, U1215 Neurocentre Magendie, Endocannabinoids and Neuroadaptation, Bordeaux, France. Université de Bordeaux, France), Beat Lutz (Institute of Physiological Chemistry and German Resilience Center, University Medical Center of the Johannes Gutenberg University Mainz, Germany) and Susana Mato (Achucarro Basque Center for Neuroscience, Science Park of the UPV/EHU, Leioa, Vizcaya, Spain) for providing the CB_1 receptor knock-out mice. This work was supported by MINECO/FEDER, UE (grant number SAF2015-65034-R to PG); The Basque Government (grant number BCG IT764-13 to PG); Red de Trastornos Adictivos, Instituto de Salud Carlos III (ISC-III) and European Regional Development Funds-European Union (ERDF-EU; grant RD16/0017/0012 to PG); PhD contract from MINECO (BES-2013-065057 to SP); Vanier Canada Graduate Scholarship (NSERC to CJF).

References

Aggleton, J.P., Brown, M.W., 1999. Episodic memory, amnesia, and the hippocampal-anterior thalamic axis. Behav. Brain Sci. 22, 425–444 discussion 444-89.

Amaral, D.G., Witter, M.P., 1989. The three-dimensional organization of the hippocampal formation: a review of anatomical data. Neuroscience 31, 571–591.

Attucci, S., Carlà, V., Mannaioni, G., Moroni, F., 2001. Activation of type 5 metabotropic glutamate receptors enhances NMDA responses in mice cortical wedges. Br. J. Pharmacol. 132, 799–806. https://doi.org/10.1038/sj.bjp.0703904.

Azad, S.C., Monory, K., Marsicano, G., Cravatt, B.F., Lutz, B., Zieglgänsberger, W., Rammes, G., 2004. Circuitry for associative plasticity in the amygdala involves endocannabinoid signaling. J. Neurosci. 24, 9953–9961. https://doi.org/10.1523/JNEUROSCI.2134-04.2004.

Bender, V.A., Bender, K.J., Brasier, D.J., Feldman, D.E., 2006. Two coincidence detectors for spike timing-dependent plasticity in somatosensory cortex. J. Neurosci. 26, 4166–4177. https://doi.org/10.1523/JNEUROSCI.0176-06.2006.

Bonilla-Del Río, I., Puente, N., Peñasco, S., Rico, I., Gutiérrez-Rodŕguez, A., Elezgarai, I., Ramos, A., Reguero, L., Gerrikagoitia, I., Christie, B.R., Nahirney, P., Grandes, P., 2019. Adolescent ethanol intake alters cannabinoid type-1 receptor localization in astrocytes of the adult mouse hippocampus. Addict. Biol. 24, 182–192. https://doi.org/10.1111/adb.12585.

Brenowitz, S.D., Regehr, W.G., 2003. Calcium dependence of retrograde inhibition by endocannabinoids at synapses onto Purkinje cells. J. Neurosci. 23, 6373–6384.

Burwell, R.D., 2000. The parahippocampal region: corticocortical connectivity. Ann. N. Y. Acad. Sci. 911, 25–42.

Busquets-Garcia, A., Oliveira da Cruz, J.F., Terral, G., Zottola, A.C.P., Soria-Gómez, E., Contini, A., Martin, H., Redon, B., Varilh, M., Ioannidou, C., Drago, F., Massa, F., Fioramonti, X., Trifilieff, P., Ferreira, G., Marsicano, G., 2018. Hippocampal CB1 receptors control incidental associations. Neuron 99, 1247–1259. e7. https://doi.org/10.1016/j.neuron.2018.08.014.

Castillo, P.E., Younts, T.J., Chávez, A.E., Hashimotodani, Y., 2012. Endocannabinoid signaling and synaptic function. Neuron 76, 70–81. https://doi.org/10.1016/j.neuron.2012.09.020.

Chávez, A.E., Chiu, C.Q., Castillo, P.E., 2010. TRPV1 activation by endogenous anandamide triggers postsynaptic long-term depression in dentate gyrus. Nat. Neurosci. 13, 1511–1518. https://doi.org/10.1038/nn.2684.

Chanda, P.K., Gao, Y., Mark, L., Btesh, J., Strassle, B.W., Lu, P., Piesla, M.J., Zhang, M.Y.,

Bingham, B., Uveges, A., Kowal, D., Garbe, D., Kouranova, E.V., Ring, R.H., Bates, B., Pangalos, M.N., Kennedy, J.D., Whiteside, G.T., Samad, T.A., 2010. Monoacylglycerol lipase activity is a critical modulator of the tone and integrity of the endocannabinoid system. Mol. Pharmacol. 78, 996–1003. https://doi.org/10.1124/mol.110.068304.
Chevaleyre, V., Castillo, P.E., 2004. Endocannabinoid-mediated metaplasticity in the hippocampus. Neuron 43, 871–881. https://doi.org/10.1016/j.neuron.2004.08.036.
Chiu, C.Q., Castillo, P.E., 2008. Input-specific plasticity at excitatory synapses mediated by endocannabinoids in the dentate gyrus. Neuropharmacology 54, 68–78. https://doi.org/10.1016/j.neuropharm.2007.06.026.
Christie, B.R., Abraham, W.C., 1994. L-type voltage-sensitive calcium channel antagonists block heterosynaptic long-term depression in the dentate gyrus of anaesthetized rats. Neurosci. Lett. 167, 41–45.
Eichenbaum, H., 2000. Hippocampus: mapping or memory? Curr. Biol. 10, R785–R787.
Eichenbaum, H., Fortin, N.J., 2005. Bridging the gap between brain and behavior: cognitive and neural mechanisms of episodic memory. J. Exp. Anal. Behav. 84, 619–629.
Eichenbaum, H., Sauvage, M., Fortin, N., Komorowski, R., Lipton, P., 2012. Towards a functional organization of episodic memory in the medial temporal lobe. Neurosci. Biobehav. Rev. 36, 1597–1608. https://doi.org/10.1016/j.neubiorev.2011.07.006.
Errington, M.L., Lynch, M.A., Bliss, T.V., 1987. Long-term potentiation in the dentate gyrus: induction and increased glutamate release are blocked by D(-)aminophosphonovalerate. Neuroscience 20, 279–284.
Fyhn, M., Molden, S., Witter, M.P., Moser, E.I., Moser, M.-B., 2004. Spatial representation in the entorhinal cortex. Science 305 (80), 1258–1264. https://doi.org/10.1126/science.1099901.
Gaffan, D., 1998. Idiothetic input into object-place configuration as the contribution to memory of the monkey and human hippocampus: a review. Exp. Brain Res. 123, 201–209.
Grandes, P., Streit, P., 1991. Effect of perforant path lesion on pattern of glutamate-like immunoreactivity in rat dentate gyrus. Neuroscience 41, 391–400.
Gutiérrez-Rodríguez, A., Puente, N., Elezgarai, I., Ruehle, S., Lutz, B., Reguero, L., Gerrikagoitia, I., Marsicano, G., Grandes, P., 2017. Anatomical characterization of the cannabinoid CB $_1$ receptor in cell-type-specific mutant mouse rescue models. J. Comp. Neurol. 525, 302–318. https://doi.org/10.1002/cne.24066.
Hargreaves, E.L., Rao, G., Lee, I., Knierim, J.J., 2005. Major dissociation between medial and lateral entorhinal input to dorsal hippocampus. Science 308, 1792–1794. https://doi.org/10.1126/science.1110449.
Hjorth-Simonsen, A., 1972. Projection of the lateral part of the entorhinal area to the hippocampus and fascia dentata. J. Comp. Neurol. 146, 219–231. https://doi.org/10.1002/cne.901460206.
Hjorth-Simonsen, A., Jeune, B., 1972. Origin and termination of the hippocampal perforant path in the rat studied by silver impregnation. J. Comp. Neurol. 144, 215–231. https://doi.org/10.1002/cne.901440206.
Hofmann, M.E., Nahir, B., Frazier, C.J., 2006. Endocannabinoid-mediated depolarization-induced suppression of inhibition in hilar mossy cells of the rat dentate gyrus. J. Neurophysiol. 96, 2501–2512. https://doi.org/10.1152/jn.00310.2006.
Hu, S.S.-J., Mackie, K., 2015. Distribution of the endocannabinoid system in the central nervous system. In: Handbook of Experimental Pharmacology, pp. 59–93. https://doi.org/10.1007/978-3-319-20825-1_3.
Huber, K.M., Sawtell, N.B., Bear, M.F., 1998. Effects of the metabotropic glutamate receptor antagonist MCPG on phosphoinositide turnover and synaptic plasticity in visual cortex. J. Neurosci. 18, 1–9.
Hunt, D.L., Puente, N., Grandes, P., Castillo, P.E., 2013. Bidirectional NMDA receptor plasticity controls CA3 output and heterosynaptic metaplasticity. Nat. Neurosci. 16, 1049–1059.
Isokawa, M., Alger, B.E., 2005. Retrograde endocannabinoid regulation of GABAergic inhibition in the rat dentate gyrus granule cell. J. Physiol. 567, 1001–1010. https://doi.org/10.1113/jphysiol.2005.094219.
Jia, Z., Lu, Y., Henderson, J., Taverna, F., Romano, C., Abramow-Newerly, W., Wojtowicz, J.M., Roder, J., 1998. Selective abolition of the NMDA component of long-term potentiation in mice lacking mGluR5 (n.d.). Learn. Mem. 5, 331–343.
Katona, I., Freund, T.F., 2012. Multiple functions of endocannabinoid signaling in the brain. Annu. Rev. Neurosci. 35, 529–558. https://doi.org/10.1146/annurev-neuro-062111-150420.
Katona, I., Urbán, G.M., Wallace, M., Ledent, C., Jung, K.-M., Piomelli, D., Mackie, K., Freund, T.F., 2006. Molecular composition of the endocannabinoid system at glutamatergic synapses. J. Neurosci. 26, 5628–5637. https://doi.org/10.1523/JNEUROSCI.0309-06.2006.
Kawamura, Y., Fukaya, M., Maejima, T., Yoshida, T., Miura, E., Watanabe, M., Ohno-Shosaku, T., Kano, M., 2006. The CB1 cannabinoid receptor is the major cannabinoid receptor at excitatory presynaptic sites in the hippocampus and cerebellum. J. Neurosci. 26, 2991–3001. https://doi.org/10.1523/JNEUROSCI.4872-05.2006.
Lafourcade, M., Elezgarai, I., Mato, S., Bakiri, Y., Grandes, P., Manzoni, O.J., 2007. Molecular components and functions of the endocannabinoid system in mouse prefrontal cortex. PLoS One 2, 1–11. https://doi.org/10.1371/journal.pone.0000709.
Lisman, J.E., Talamini, L.M., Raffone, A., 2005. Recall of memory sequences by interaction of the dentate and CA3: a revised model of the phase precession. Neural Network. 18, 1191–1201. https://doi.org/10.1016/j.neunet.2005.08.008.
Lutz, B., Marsicano, G., Maldonado, R., Hillard, C.J., 2015. The endocannabinoid system in guarding against fear, anxiety and stress. Nat. Rev. Neurosci. 16, 705–718. https://doi.org/10.1038/nrn4036.
Mannaioni, G., Marino, M.J., Valenti, O., Traynelis, S.F., Conn, P.J., 2001. Metabotropic glutamate receptors 1 and 5 differentially regulate CA1 pyramidal cell function. J. Neurosci. 21, 5925–5934.
Marsicano, G., Lutz, B., 1999. Expression of the cannabinoid receptor CB1 in distinct neuronal subpopulations in the adult mouse forebrain. Eur. J. Neurosci. 11, 4213–4225.
Monday, H.R., Younts, T.J., Castillo, P.E., 2018. Long-term plasticity of neurotransmitter release: emerging mechanisms and contributions to brain function and disease. Annu. Rev. Neurosci. 41, 299–322. https://doi.org/10.1146/annurev-neuro-080317-062155.
Monory, K., Massa, F., Egertová, M., Eder, M., Blaudzun, H., Westenbroek, R., Kelsch, W., Jacob, W., Marsch, R., Ekker, M., Long, J., Rubenstein, J.L., Goebbels, S., Nave, K.-A., During, M., Klugmann, M., Wölfel, B., Dodt, H.-U., Zieglgänsberger, W., Wotjak, C.T., Mackie, K., Elphick, M.R., Marsicano, G., Lutz, B., 2006. The endocannabinoid system controls key epileptogenic circuits in the Hippocampus. Neuron 51, 455–466. https://doi.org/10.1016/j.neuron.2006.07.006.
Neyman, S., Manahan-Vaughan, D., 2008. Metabotropic glutamate receptor 1 (mGluR1) and 5 (mGluR5) regulate late phases of LTP and LTD in the hippocampal CA1 region in vitro. Eur. J. Neurosci. 27, 1345–1352. https://doi.org/10.1111/j.1460-9568.2008.06109.x.
Peñasco, S., Puente, N., Ramos, A., Royo, N., Gutiérrez-Rodríguez, A., Bonilla-Del Río, I., Reguero, L., Canduela, M.J., Mendizabal-Zubiaga, J., Rodrígez de Fonseca, F., Suárez, J., Elezgarai, I., Grandes, P., 2015. Alteration of the endocannabinoid-dependent synaptic plasticity in adult brain after ethanol exposure of mice during adolescence. In: 25 Th Annual Symposium of the INTERNATIONAL CANNABINOID RESEARCH SOCIETY, pp. 17.
Pertwee, R.G., 2015. In: Pertwee, R.G. (Ed.), Endocannabinoids and Their Pharmacological Actions. Springer International Publishing, Cham, pp. 1–37. Endocannabinoids. https://doi.org/10.1007/978-3-319-20825-1_1.
Petersen, R.P., Moradpour, F., Eadie, B.D., Shin, J.D., Kannangara, T.S., Delaney, K.R., Christie, B.R., 2013. Electrophysiological identification of medial and lateral perforant path inputs to the dentate gyrus. Neuroscience 252, 154–168. https://doi.org/10.1016/j.neuroscience.2013.07.063.
Piomelli, D., 2003. The molecular logic of endocannabinoid signalling. Nat. Rev. Neurosci. 4, 873–884. https://doi.org/10.1038/nrn1247.
Puente, N., Cui, Y., Lassalle, O., Lafourcade, M., Georges, F., Venance, L., Grandes, P., Manzoni, O.J., 2011. Polymodal activation of the endocannabinoid system in the extended amygdala. Nat. Neurosci. 14, 1542–1547. https://doi.org/10.1038/nn.2974.
Puente, N., Reguero, L., Elezgarai, I., Canduela, M.J., Mendizabal-Zubiaga, J., Ramos-Uriarte, A., Fern??ndez-Espejo, E., Grandes, P., 2015. The transient receptor potential vanilloid-1 is localized at excitatory synapses in the mouse dentate gyrus. Brain Struct. Funct. 220, 1187–1194. https://doi.org/10.1007/s00429-014-0711-2.
Reagh, Z.M., Yassa, M.A., 2014. Object and spatial mnemonic interference differentially engage lateral and medial entorhinal cortex in humans. Proc. Natl. Acad. Sci. Unit. States Am. 111, E4264–E4273. https://doi.org/10.1073/pnas.1411250111.
Rico-Barrio, I., Peñasco, S., Puente, N., Ramos, A., Fontaine, C.J., Reguero, L., Giordano, M.E., Buceta, I., Terradillos, I., Lekunberri, L., Mendizabal-Zubiaga, J., Rodríguez de Fonseca, F., Gerrikagoitia, I., Elezgarai, I., Grandes, P., 2018. Cognitive and neurobehavioral benefits of an enriched environment on young adult mice after chronic ethanol consumption during adolescence. Addict. Biol. https://doi.org/10.1111/adb.12667.
Ruehle, S., Remmers, F., Romo-Parra, H., Massa, F., Wickert, M., Wörtge, S., Häring, M., Kaiser, N., Marsicano, G., Pape, H.-C., Lutz, B., 2013. Cannabinoid CB1 receptor in dorsal telencephalic glutamatergic neurons: distinctive sufficiency for hippocampus-dependent and amygdala-dependent synaptic and behavioral functions. J. Neurosci. 33, 10264–10277. https://doi.org/10.1523/JNEUROSCI.4171-12.2013.
Scharfman, H.E., Myers, C.E., 2013. Hilar mossy cells of the dentate gyrus: a historical perspective. Front. Neural Circuits 6, 106. https://doi.org/10.3389/fncir.2012.00106.
Schlosburg, J.E., Blankman, J.L., Long, J.Z., Nomura, D.K., Pan, B., Kinsey, S.G., Nguyen, P.T., Ramesh, D., Booker, L., Burston, J.J., Thomas, E.A., Selley, D.E., Sim-Selley, L.J., Liu, Q.S., Lichtman, A.H., Cravatt, B.F., 2010. Chronic monoacylglycerol lipase blockade causes functional antagonism of the endocannabinoid system. Nat. Neurosci. 13, 1113–1119. https://doi.org/10.1038/nn.2616.
Sjöström, P.J., Turrigiano, G.G., Nelson, S.B., 2003. Neocortical LTD via coincident activation of presynaptic NMDA and cannabinoid receptors. Neuron 39, 641–654.
Suzuki, W.A., Miller, E.K., Desimone, R., 1997. Object and place memory in the macaque entorhinal cortex. J. Neurophysiol. 78, 1062–1081. https://doi.org/10.1152/jn.1997.78.2.1062.
Uchigashima, M., Yamazaki, M., Yamasaki, M., Tanimura, A., Sakimura, K., Kano, M., Watanabe, M., 2011. Molecular and morphological configuration for 2-arachidonoylglycerol-mediated retrograde signaling at mossy cell-granule cell synapses in the dentate gyrus. J. Neurosci. 31, 7700–7714. https://doi.org/10.1523/JNEUROSCI.5665-10.2011.
Wang, W., Jia, Y., Pham, D.T., Palmer, L.C., Jung, K.-M., Cox, C.D., Rumbaugh, G., Piomelli, D., Gall, C.M., Lynch, G., 2018. Atypical endocannabinoid signaling initiates a new form of memory-related plasticity at a cortical input to Hippocampus. Cerebr. Cortex 28, 2253–2266. https://doi.org/10.1093/cercor/bhx126.
Wang, W., Trieu, B.H., Palmer, L.C., Jia, Y., Pham, D.T., Jung, K.-M., Karsten, C.A., Merrill, C.B., Mackie, K., Gall, C.M., Piomelli, D., Lynch, G., 2016. A primary cortical input to Hippocampus expresses a pathway-specific and endocannabinoid-dependent form of long-term potentiation. eNeuro 3. https://doi.org/10.1523/ENEURO.0160-16.2016.
Yasuda, H., Huang, Y., Tsumoto, T., 2008. Regulation of excitability and plasticity by endocannabinoids and PKA in developing hippocampus. Proc. Natl. Acad. Sci. U.S.A. 105, 3106–3111. https://doi.org/10.1073/pnas.0708349105.
Yoshida, T., Fukaya, M., Uchigashima, M., Miura, E., Kamiya, H., Kano, M., Watanabe, M., 2006. Localization of diacylglycerol lipase- around postsynaptic spine suggests close proximity between production site of an endocannabinoid, 2-Arachidonoylglycerol, and presynaptic cannabinoid CB1 receptor. J. Neurosci. 26, 4740–4751. https://doi.org/10.1523/JNEUROSCI.0054-06.2006.